Journal of Marine Systems 76 (2009) 417–432

Contents lists available at ScienceDirect

Journal of Marine Systems

journal homepage: www.elsevier.com/locate/jmarsys

From suspended particles to strata: The fate of terrestrial substances in the Gaoping (Kaoping) submarine canyon

James T. Liu [a,*], Jia-Jang Hung [a], Hui-Ling Lin [a], Chih-An Huh [b], Chon-Lin Lee [c], Ray T. Hsu [a], Ya-Wen Huang [b], Joel C. Chu [a]

[a] Institute of Marine Geology and Chemistry, National Sun Yat-sen University, Kaohsiung, Taiwan 80424, ROC
[b] Institute of Earth Sciences, Academia Sinica, Taipei, Taiwan 11529, ROC
[c] Department of Marine Environment and Engineering, National Sun Yat-sen University, Kaohsiung, Taiwan 80424, ROC

ARTICLE INFO

Article history:
Received 31 May 2007
Received in revised form 3 January 2008
Accepted 24 January 2008
Available online 23 August 2008

Keywords:
Submarine canyon
Sediment trap
Particle dynamics
Source-to-sink
Particle size
Lithogenic sediment
Post-depositional disturbance

ABSTRACT

The river–sea system consisting of the Gaoping (new spelling according to the latest government's directive, formerly spelled Kaoping) River (KPR), shelf, and Submarine Canyon (KPRSC) located off southern Taiwan is an ideal natural laboratory to study the source, pathway, transport, and fate of terrestrial substances. In 2004 during the flood season of the KPR, a system-wide comprehensive field experiment was conducted to investigate particle dynamics from a source-to-sink perspective in the KPRSC with the emphasis on the effect of particle size on the transport, settling, and sedimentation along the pathway. This paper reports the findings from (1) two sediment trap moorings each configured with a Technicap PPS 3/3 sediment trap, and an acoustic current meter (Aquadopp); (2) concurrent hydrographic profiling and water sampling was conducted over 8 h next to the sediment trap moorings; and (3) box-coring in the head region of the submarine canyon near the mooring sites. Particle samples from sediment traps were analyzed for mass fluxes, grain-size composition, total organic carbon (TOC) and nitrogen (TN), organic matter (OM), carbonate, biogenic opal, polycyclic aromatic hydrocarbon (PAH), lithogenic silica and aluminum, and foraminiferal abundance. Samples from box cores were analyzed for grain-size distribution, TOC, particulate organic matter (POM), carbonate, biogenic opal, water content, and $^{210}Pb_{ex}$. Water samples were filtered through 500, 250, 63, 10 μm sieves and 0.4 μm filter for the suspended sediment concentration of different size-classes. Results show that the river and shelf do not supply all the suspended particles near the canyon floor. The estimated mass flux near the canyon floor exceeds 800 g/m^2/day, whose values are 2–7 times higher than those at the upper rim of the canyon. Most of the suspended particles in the canyon are fine-grained (finer than medium silt) lithogenic sediments whose percentages are 90.2% at the upper rim and 93.6% in the deeper part of the canyon.

As suspended particles settle through the canyon, their size-composition shows a downward fining trend. The average percentage of clay-to-fine-silt particles (0.4–10 μm) in the water samples increases from 22.7% above the upper rim of the canyon to 56.0% near the bottom of the canyon. Conversely, the average percentage of the sand-sized (>63 μm) suspended particles decreases downward from 32.0% above the canyon to 12.0% in the deeper part of the canyon. Correspondingly, the substrate of the canyon is composed largely of hemipelagic lithogenic mud. Parallel to this downward fining trend is the downward decrease of concentrations of suspended nonlithogenic substances such as TOC and PAH, despite of their affinity to fine-grained particles.

On the surface of the canyon, down-core variables (grain size, $^{210}Pb_{ex}$ activity, TOC, water content) near the head region of the canyon show post-depositional disturbances such as hyperpycnite and turbiditic deposits. These deposits point to the occurrences of erosion and deposition related to high-density flows such as turbidity currents, which might be an important process in submarine canyon sedimentation.

* Corresponding author. Fax: +886 7 525 5130.
E-mail address: james@mail.nsysu.edu.tw (J.T. Liu).

0924-7963/$ – see front matter © 2008 Elsevier B.V. All rights reserved.
doi:10.1016/j.jmarsys.2008.01.010

1. Introduction

Many submarine canyons are integral parts of river–sea transport systems, which are also preferential conduits for the delivery, transport, and trapping of river-borne substances (Kudrass et al., 1998; Granata et al., 1999; Mullenbach and Nittrouer, 2000; Palanques et al., 2005a,b; Liu et al., 2006) to the open sea. Liu and Lin (2004) classify river–sea transport systems containing submarine canyons into two major types based on geographic configuration of the river mouth and the canyon. In their scheme, the difference between the two types is whether the river mouth (point source for river-borne substances) and the head of the canyon (beginning of the sediment conduit and trap) are separated by a shelf.

Submarine canyons that directly receive sediment from rivers near and far have rapid deposition of fluvial sediment (Mullenbach and Nittrouer, 2000), are effective temporary traps of fluvial sediment during the flood season (Kudrass et al., 1998); and have high mass fluxes (Palanques et al., 2005a; Liu et al., 2006). In recent years there have been numerous particle flux studies in submarine canyons (Liu and Lin, 2004; Palanques et al., 2005a,b; Liu et al., 2006) and on open continental margins (Hung and Chung, 1998; Miserocchi et al., 1999; Chung and Hung, 2000; Fabres et al., 2002; Timothy et al., 2003; Sanchez-Vidal et al., 2005). Their findings are similar that most particle fluxes increase with depth and suspended particles are predominantly lithogenic, whose percentage also increases with depth (Miserocchi et al., 1999; Palanques et al., 2005a). Common nonlithogenic constituents measured in the particle fluxes/dynamics studies include (not exclusively) calcium carbonate, organic carbon, biogenic opal, organic matter, and some stable isotopes such as $\delta^{13}C$, $\delta^{15}N$ and radial isotopes such as $^{210}Pb_{ex}$.

As the particles settle through the water column, biogeochemical transformation such as degradation, decomposition, and remineralization of organic and biogenic matter takes place (Fabres et al., 2002; Lund-Hansen et al., 2004; Sanchez-Vidal et al., 2005). The result is the decreasing percentage/flux of organic matter and increase C/N ratio with depth. As the particles settle, organic matter could be diluted by lithogenic particles as well (Bonnin et al., 2002; Masque et al., 2003; Liu and Lin, 2004). Near the canyon or shelf floor, a benthic nepheloid layer (BNL) often exists (Bonnin et al., 2002; Liu et al., 2002; Masque et al., 2003) in which the particles could come from downward settling, rebound material in the water column and resuspended material from the floor (Bonnin et al., 2002). Bottom nepheloid layers are involved in the supply of significant fraction of sediment to the deep (Masque et al., 2003) and they could be related to the breaking of internal waves (Gardner, 1989; Puig et al., 2004).

Despite of downward particle fluxes, submarine canyons are dominated by erosional processes (Mulder et al., 2001) related to particle-laden gravity currents (turbidity currents). Turbidity currents have been observed in Monterey Canyon possibly induced by storms (Xu et al., 2004) and in Zaire submarine valley (Khripounoff et al., 2003). Liu et al. (2006) also report an intense down-canyon flushing event of high SSC (suspended sediment concentration) during a typhoon near the floor of the Gaoping (formerly spelled Kaoping) Submarine Canyon. Gravity currents such as turbidity currents and hyperpycnal flows are probably important transport agents to move sediment down-canyon, they are also geological agents creating noticeable deposits in the stratigraphic sequences (turbidites and hyperpycnites) on the sea floor (Mulder et al., 2001, 2003; Masque et al., 2003).

Submarine canyons are complex depositional systems. They are fed by rivers, ocean currents, waves, and tides. Their particle inputs come from a wide range of terrestrial (lithogenic), reworked, and marine (biogenic) sources. The sinking particles in the canyon interior are subject to physical and biogeochemical processes that affect their distribution and properties. Once the particles settle to the canyon floor, they are subject to episodes of erosion and transport in a stepwise fashion. Furthermore, a wide range of space scales are involved from the drainage basin of the feeder river, the width of the shelf, and the terminal submarine fan or ocean basin. On the time scale, forcing and response processes range from seconds, to tidal and subtidal, to seasonal, decadal and beyond. Yet, there has not been a comprehensive study of such a depositional system from the source-to-sink perspective. Furthermore, no study has been done on the effect of the particle size along the source-to-sink pathway and its biogeochemical implications. Therefore, the objective of this study is to examine the effects of the particle size on the source, transport, transformation, and deposition of suspended sediment in a submarine canyon. Our goal is to present a conceptual model that integrates the physical, biogeochemical, and sedimentological aspects in the sedimentation process from suspended particles to the formation of strata through the grain size along the shelf-canyon pathway.

2. Study area and background

The Gaoping (Kaoping) Submarine Canyon located off southern Taiwan as part of the river–sea system of the Gaoping (Kaoping) River (KPR), shelf, and Submarine Canyon (KPRSC), is an active two-way conduit between the Taiwan orogen and South China Sea (Liu et al., 2006). Previously, Liu et al. (2002) using several statistical techniques on grain-size distribution patterns and hydrographic surveys, reveal that (1) the Gaoping (Kaoping) Submarine Canyon (KPSC) interrupts the littoral sediment transport on the shelf, (2) both up-canyon and down-canyon sediment transport directions exist inside the KPSC, (3) a depocenter is inferred in the head region of the canyon where the surficial mud content is over 90% by weight, and (4) spots of high suspended sediment concentration (SSC) in the BNL is likely related to the propagation of internal tide. They hypothesized that the trapping of internal tidal energy caused the formation of the observed depocenter.

In order to physically verify the existence of the depocenter, and understand the sediment dynamics involved, in the ensuing studies sediment trap moorings were deployed at the hypothesized depocenter location in the flood seasons of 2000 (for lower part of the canyon, Liu and Lin, 2004), 2002 (partially successful, Liu et al., 2006), and 2004 (this study). Liu and Lin (2004) show that river plume dynamics and the coastal wind field largely control the delivery of terrigenous fine-grained sediment to the canyon. Inside the canyon, the 'behavior' of suspended lithogenic and nonlithogenic particles of different sizes can be differentiated into a coarse-

grained group (sand), which forms the 'drop-in' population; and a fine-grained group (mud), which forms the 'standing' population. The coarse-grained group is delivered directly to the canyon by the river effluent, and by wave resuspension of the shelf substrate. During the study period, the net transport of suspended particles near the canyon floor was up-canyon mostly by tidal currents, whose direction was also modulated by spring/neap tide.

Recently, Liu et al. (2006) discovered that typhoons could play an important role in the submarine canyon dynamics. In their case study, the KPRSC is impacted by a typhoon event in two phases. The distal phase starts when the typhoon is still hundreds of kilometres away, in which the influence of typhoon is mainly seen in the marine signals from the distal South China Sea (Lin et al., 2005), and indirect dilution of terrestrial signals (TOC and $\delta^{13}C$) by signals of marine origin and reworked substrate (Liu et al., 2006). In the ensuing proximal phase when the typhoon gets closer, there is the enhancement of local forcings such as high waves, river runoff and sediment discharge (Liu et al., 2006). In the above two phases the deliveries of both terrestrial and marine substances are amplified. Liu et al. (2006) also observed one occurrence that a momentary down-canyon flushing of suspended particles near the canyon floor took place during the typhoon event, which might trigger turbidity currents that lead to turbiditic deposits. Therefore, they assert that typhoons are not only physical agents for enhanced delivery of terrestrial/nonterrestrial substances to the system, but are also geological agents for triggering canyon slumping and debris flow that eventually leaves deposits on the canyon floor.

All the previous studies have provided a good foundation for the preliminary understanding of the delivery and transport of terrestrial and marine substances in the KPSC. This study takes one step further to investigate the fate of terrestrial and marine substances in the head region of the KPSC from the source-to-sink perspective. Special emphasis has been given to the effect of grain size and its biogeochemical implications in the transport, settling, and accumulation of suspended sediment in the head region of KPSC.

3. Field experiments

Between May 25 and June 25, 2004 a comprehensive system-wide field experiment was carried out during the flood season of the river. The experiment consisted of simultaneous deployments of an instrumented tetrapod in the lower reaches of the KPR (not presented in this paper), two taut-line moorings in the head region of the KPSC (Fig. 1a), and shipboard coring and hydrographic profiling and water sampling in the head region of the canyon and on the Gaoping shelf and slope. Because of insufficient floatation, the two moorings were subject to noticeable tilt (Lee and Liu, 2006).

During the one-month deployment, the study area was mildly affected by Typhoon Conson that passed by off the southern tip of Taiwan on the Pacific Ocean side in a NE direction (Fig. 1b). Although this typhoon did not make landfall on Taiwan, it did influence the coastal wind and wave fields in the study area (Fig. 2a, b) as indicated by the brief period of northerly winds instead of southwesterly summer monsoon winds and a high wave energy event (Fig. 2a, b) around June 8 when the center of the typhoon was the closest to the study area (Fig. 1b). However, even the precipitation increased in the two-week period centered around this typhoon, the daily KPR runoff and suspended sediment flux recorded at the Liling Bridge gauging station shows a drop on June 7 (Fig. 2c).

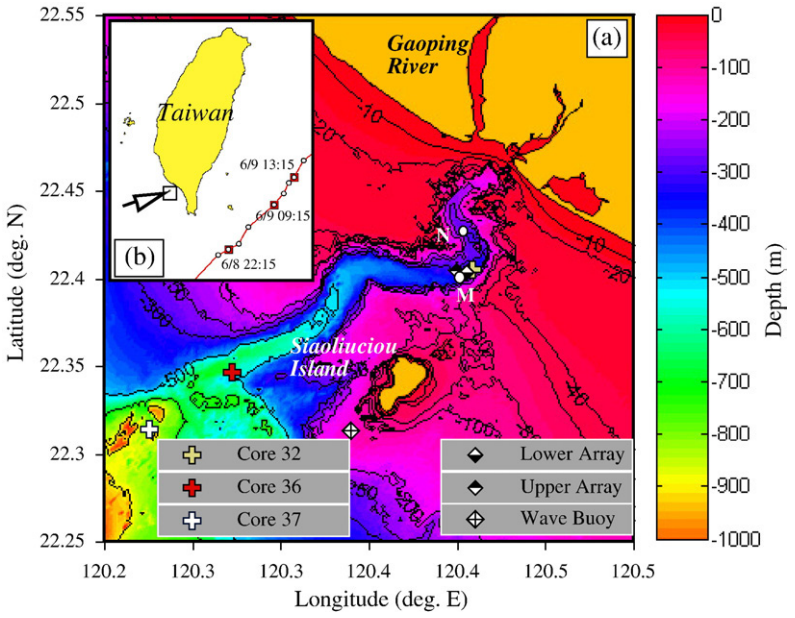

Fig. 1. (a) Bathymetric map of the study area indicating locations of the sediment trap moorings in the Gaoping (Kaoping) Submarine Canyon, wave buoy on the shelf, and box-coring sites. The two circles indicate the hydrographic stations (M and N) where the hydrographic profiling and water samples were carried out. Depth contours are in meters based on the Keelung mean sea level (data provided by the National Center for Ocean Research). (b) The insert is a larger-scaled map of Taiwan showing the location of the study area and part of the time-annotated track of Typhoon Conson.

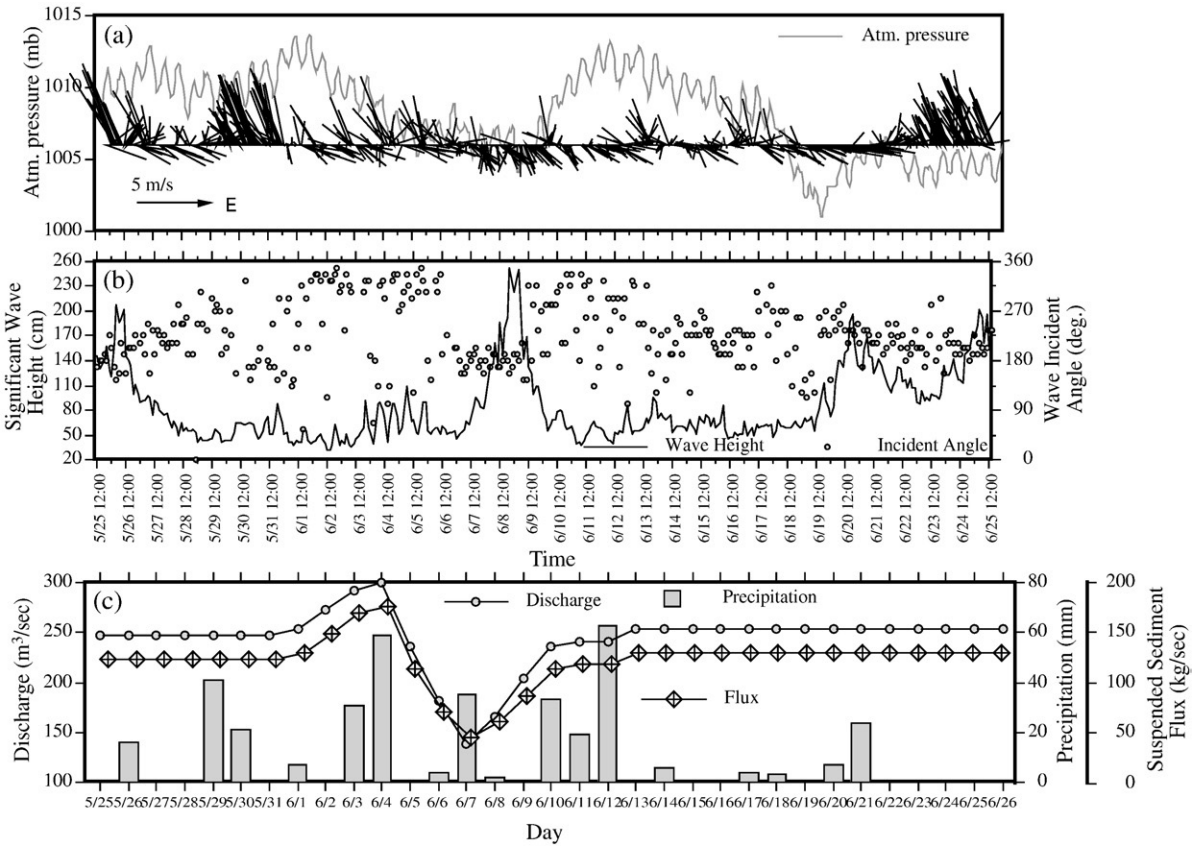

Fig. 2. Environmental conditions during the field experiment including (a) hourly measurements of the atmospheric pressure and wind (stick diagram plotted according to the oceanographic convention) recorded on the Siaoliuciou (formerly spelled Hsiao-liu-chiu) Island; (b) bi-hourly measurements of the wave field by a wave buoy offshore of Siaoliuciou Island; and (c) daily runoff, suspended sediment flux from the gauging station at Liling Bridge (about 34 km from the mouth of KPR, and daily precipitation recorded at Sandimen Weather Station in the middle reaches of KPR.

3.1. Taut-line sediment trap arrays

The two sediment trap moorings were configured to make process–response and particle dynamics observations at the upper rim (approximately 260 m from the canyon floor) and near the canyon floor (approximately 30 m from the bottom) of the KPSC (Fig. 1a). This paper only presents the observations from these two levels of acoustic current meters (Aquadopp), and two cylindrical sediment trap (Technicap PPS 3/3), which has been widely used for particle flux studies (Hung and Chung, 1998; Miserocchi et al., 1999; Fabres et al., 2002; Sanchez-Vidal et al., 2005; Palanques et al., 2005a; Liu et al., 2006). The descriptions of the configuration of the two sediment trap moorings are given in Lee and Liu (2006), they will not be repeated here. Each of the 12 collecting cups in the sediment traps was programmed to sample for 60 h.

3.2. Hydrographic profiling and water sampling

On June 18, 2004 for 8 h (roughly between 10 am and 6 pm) largely during the ebbing tide on the shelf, hourly CTD including light transmission (Sea Bird SBE 9/11), and LISST-100 (not presented in this paper) profiling was conducted on board R/V Ocean Researcher III (OR-III) at two locations (St. N, M) near the deployed moorings (Fig. 1a). On each cast, water samples (10 L each) were taken at discrete depths. The water samples were later filtered for SSC at the laboratory. Because of the time constraint, water samples were taken at hours 1, 2, 4, 6, and 8 during the 8-hour period.

3.3. Box-coring in KPSC on board OR-III on Cruise #732

A Smith Macintyre box core was used to obtain the substrate samples of the study area. Multiple subsamples of each box core were taken on deck of R/V OR-III by pressing PVC tubings into the sediment in the core. One subsample was kept for archive.

4. Analytical methods

4.1. Sediment trap samples

4.1.1. Grain-size analysis

The same procedure described by Liu and Lin (2004) for sample preparation was used before the sample was analyzed for the grain-size distribution using a laser particle analyzer (Coulter LS100). For the convenience for later cross-comparison with filtered suspended particle-size data, the output of LS100 was grouped into the following size-classes: 0.4–10, 10–63, and >63 μm.

To obtain the size-composition of approximately the lithogenic component of the sediment samples, the following was removed sequentially from the subsample:

organic substances, $CaCO_3$, and biogenic opal before the particle-size analysis. To start, the subsample was added with a dispersant of 5% of $NaPO_5$ solution and placed on vibrating mixer for 5 min to disintegrate flocculated and aggregated substances. The sample was left overnight to allow the particles to settle. After removing the residual liquid, the sample was washed and dried at 60 °C in the oven.

In the following step to remove organic substances, 0.5 g of the sample was put into the centrifuge tube and weighed. The sample was added with 10 ml of 37% H_2O_2, put on vibrator for 30 min, and left for one day, and then centrifuged at 6000 rpm for 5 min and drained. To remove $CaCO_3$, 30 ml of 0.5 M HCl was added to the sample, put in vibrator to 30 min and then left for about 5 days until the chemical reaction was complete. Then, the following procedure was repeated 3 times, that the sample was centrifuged at 6000 rpm for 5 min, drained, and washed with distilled deionized water (DDW) and drained.

To remove the biogenic opal, 38 ml of 0.5 M NaOH was added to the sample. The sample was then put in vibrator for 30 min. The sample was then put in a hot-water bath at 85 °C for 5 h. During this period, the sample was taken out to mix twice. Afterwards, the sample was centrifuged at 6000 rpm for 5 min, and drained. Then the sample was washed with DDW, centrifuged, and drained.

Finally, the treated samples were prepared for the particle analyzer following the same procedures as the untreated samples described before. The output of the LS100 was also grouped into the same 3 size-classes.

4.1.2. Total organic carbon (TOC) and nitrogen (TN) and the calculations of OC/IC, C/N

Each sediment sample was first screened through a nylon sieve to remove particles bigger than 1 mm. A portion of the sediment sample was washed with Milli-Q water to remove any remaining sea salt and then dried in an oven at 60 °C for at least 24 h. The dried sample was ground to powder using an agate mortar and pestle before further analyzing the contents of organic carbon and trace metals. Total organic carbon (TOC) and nitrogen (TN) were determined with a C/N/S analyzer (Fisons NCS 1500) after removing the inorganic carbon with hydrochloric acid (Hung et al., 2000). Total inorganic carbon (TIC) was determined from the difference between total carbon (TC) and TOC. Atomic ratios of TOC and TIC (OC/IC) and organic carbon and nitrogen (C/N) are estimated respectively.

4.1.3. Analysis of organic matter (OM), carbonate, and biogenic opal

The OM content was assumed to be OC (organic carbon) multiplied by 2 (Monaco et al., 1990). The carbonate content was calculated by multiplying the inorganic carbon (difference between TC and POC) by 8.33 (Monaco et al., 1990). Apparent biogenic opal was determined using a colorimetric method modified from Mortlock and Froelich (1989) after extraction with 0.5 M NaOH at 85 °C for 5 h. Nonbiogenic Si extracted by the method was estimated from extracted Al determined with flameless atomic absorption spectrometry (Perkin-Elmer 5100PC HGA-600). Biogenic opal was then estimated by subtracting nonbiogenic Si from apparent biogenic Si (Leinen, 1977).

4.1.4. Polycyclic aromatic hydrocarbon (PAH)

Details of analytical procedure for PAH could be found in Ko et al. (2007). A portion of the sediment was grounded with sufficient quantity of anhydrous sodium sulphate (Merck) to obtain a mass of dry powder. This powder mass was Soxhlet extracted for 24 h with dichloromethane. The extract volume then was reduced to ~1.5 ml by rotary evaporator and then fractionated through an aluminum oxide column (8 g, 6.0% deactivated with Milli-Q water) to remove polar interferences with the aid of 35 ml petroleum ether. The extract was concentrated to ~5 ml by rotary evaporator and further blown down to ~1 ml under a purified nitrogen stream (99.99%, purified by activated carbon column) prior to gas chromatograph mass spectrometry (GC-MS) analysis.)

4.1.5. Lithogenic silica and aluminum

Lithogenic silica was measured from the difference between total silica and biogenic silica (opal). The total Si and Al were determined by weighting the ground sediment into a microwave Teflon bottle, digested with mixed superpure acids (HNO_3:HCl:HF=3:3:4), and heated stepwise (stage 1: 420 W, 30 min; stage 2: 600 W, 60 min) by a microwave oven (CEM 2000). The digested solution was diluted with DDW and then Si and Al were analyzed with atomic absorption spectrometry. Biogenic silica was determined according to the method described in Section 4.1.1. for opal.

4.1.6. Foraminiferal abundance

Freeze dried samples were wet-sieved through a 63 μm sieve. The sand (>63 μm) fraction residue was collected, dried and then weighed. The weight percent of the coarse fraction was calculated by dividing the weight of the sand fraction by the weight of the original sample. All foraminiferal shells, both planktonic and benthic, were picked from the coarse fractions that were greater than 125 μm for faunal census. Shell concentration is calculated as numbers of individuals per gram of dry sediment (#/g).

Table 1
The analyzed parameters and their sampling intervals

	OR-III 732 Core #32	OR-III 732 Core #36	OR-III 732 Core #37
Water content (MSCL)	1 cm (0–38 cm)	NA	1 cm (0–43 cm)
Grain size	2 cm (0–30 cm), 5 cm (30–90 cm)	2 cm (0–20 cm), 5 cm (20–35 cm)	2 cm (0–20 cm), 5 cm (20–40 cm)
TOC	2 cm (0–30 cm), 5 cm (30–90 cm)	2 cm (0–42 cm)	NA
POM, carbonate, biogenic opal	2 cm (0–30 cm), 5 cm (30–90 cm)	NA	NA
$^{210}Pb_{ex}$	2 cm (0–38 cm)	2 cm (0–42 cm)	2 cm (0–42 cm)

NA: not analyzed.

4.2. Grain-size analyses of water samples from hydrographic profiling

For each water sample, the entire 10 L jug was first filtered in one setting through two stainless steel sieves of 500 and 250 μm mesh sizes and there was no retention on these sieves. The residue was filtered with 63 and 10 μm nylon sieves, and then 0.4 μm GE/C filter. Suspended sediment concentration in mg/l was subsequently measured for the following three size-classes: 0.4–10, 10–63, and >63 μm.

4.3. Surface (core-top) samples analyses

Three box cores (#32, 36, 37, Fig. 1a) taken on OR-III Cruise #732 were analyzed for this study. The analyzed parameters and their sampling intervals are listed in Table 1. The analysis methods for grain size, TOC, POM, carbonate, and biogenic opal were the same for the sediment trap samples. The $^{210}Pb_{ex}$ was analyzed using the same procedure described by Huh et al. (2004, 2006).

5. Results

5.1. Rectified flows at the upper rim and lower part of KPSC

The progressive vector of the rectified hourly flow at the upper rim of the canyon shows northwesterly (alongshore) long-term transport superimposed by short-term tidal oscillations during the first spring tide (Fig. 3a) similar to what Liu et al. (2006) reported. The flow veered toward the shore during the following neap tide. During the second spring tide the flow was more offshore-oriented than alongshore. Subsequently, the stick plot of the mean flow averaged over the 60-hour period corresponding to each collecting cup in the sediment trap at the upper rim show strong alongshore orientation during the first half part of the experiment and lack of orientation in the second part of the experiment (Fig. 3b).

In the deeper part of the canyon, it is clear that the short-term tidal flows are topographically steered to follow the canyon axis at the mooring site (Fig. 3a). The net movement of the flow is in the down-canyon direction as shown clearly in the stick plot of the averaged (over 60 h) flow, which is controlled by the spring tides (Fig. 3c).

5.2. Particle comparisons between the upper and lower traps

5.2.1. Collected weight, mass flux, grain-size composition, and nonlithogenic components

A major function for the use of sediment trap is to estimate the particle mass fluxes in the ocean assuming that the particles collected by the sediment trap were settling particles from above. Due to the complication caused by the tilt of the moorings in this study (Lee and Liu, 2006), one cannot be sure

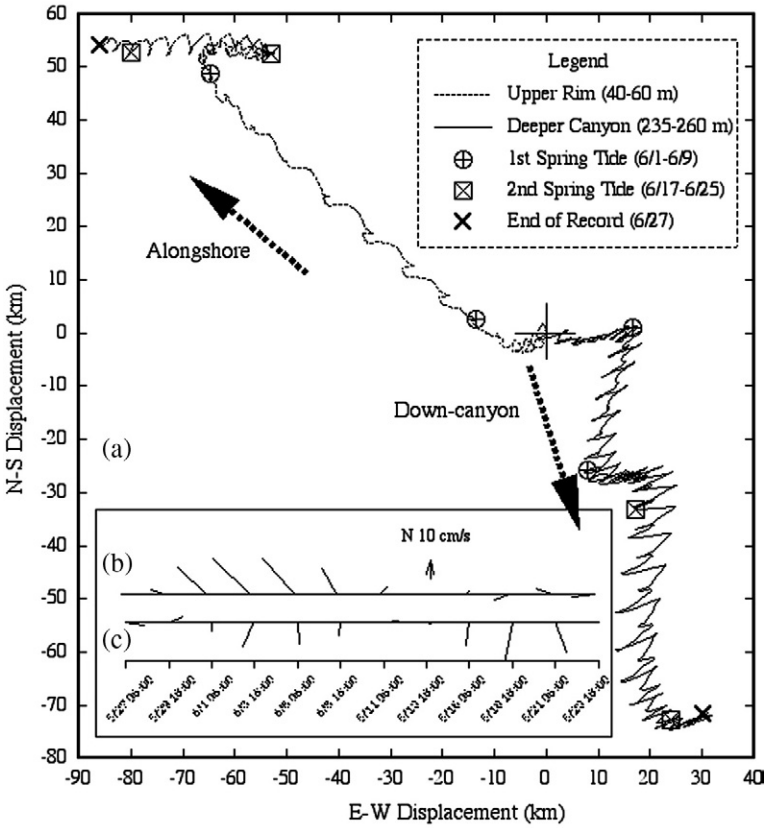

Fig. 3. (a) Progress vector plot of the rectified hourly flows at the upper rim and deeper part of the submarine canyon, respectively. The origin (indicated by the cross) is the beginning of the two synoptic records. The insert is the stick diagram of the flow averaged over the 60-hour period corresponding to each collecting cup of the upper (b) and lower (c) sediment traps.

that particles collected by the sediment traps are solely from settling. Nevertheless, the flux (collecting rate) of each cup was estimated to provide basis for comparison with each other and with previous flux measurements in this region (Liu et al., 2006). The unadjusted flux was estimated by dividing the collected dry weight (Fig. 4a, e) by the opening area of the trap unadjusted for the tilt and by the 60-hour collecting period. The adjusted flux was estimated by dividing the dry weight by the 'effective collecting area' adjusted for the tilt (opening area multiplied by the cosine of the tilt angle). The results show the difference between unadjusted and adjusted fluxes is greater for the upper trap than for the lower trap (Fig. 4a, e) since the upper trap experienced greater tilt (Lee and Liu, 2006). At the deeper part of the submarine canyon, the adjusted fluxes at spring tide exceeded 800 g/m^2/day (Fig. 4a), which is comparable to previous measurements (Liu et al., 2006). At the canyon's

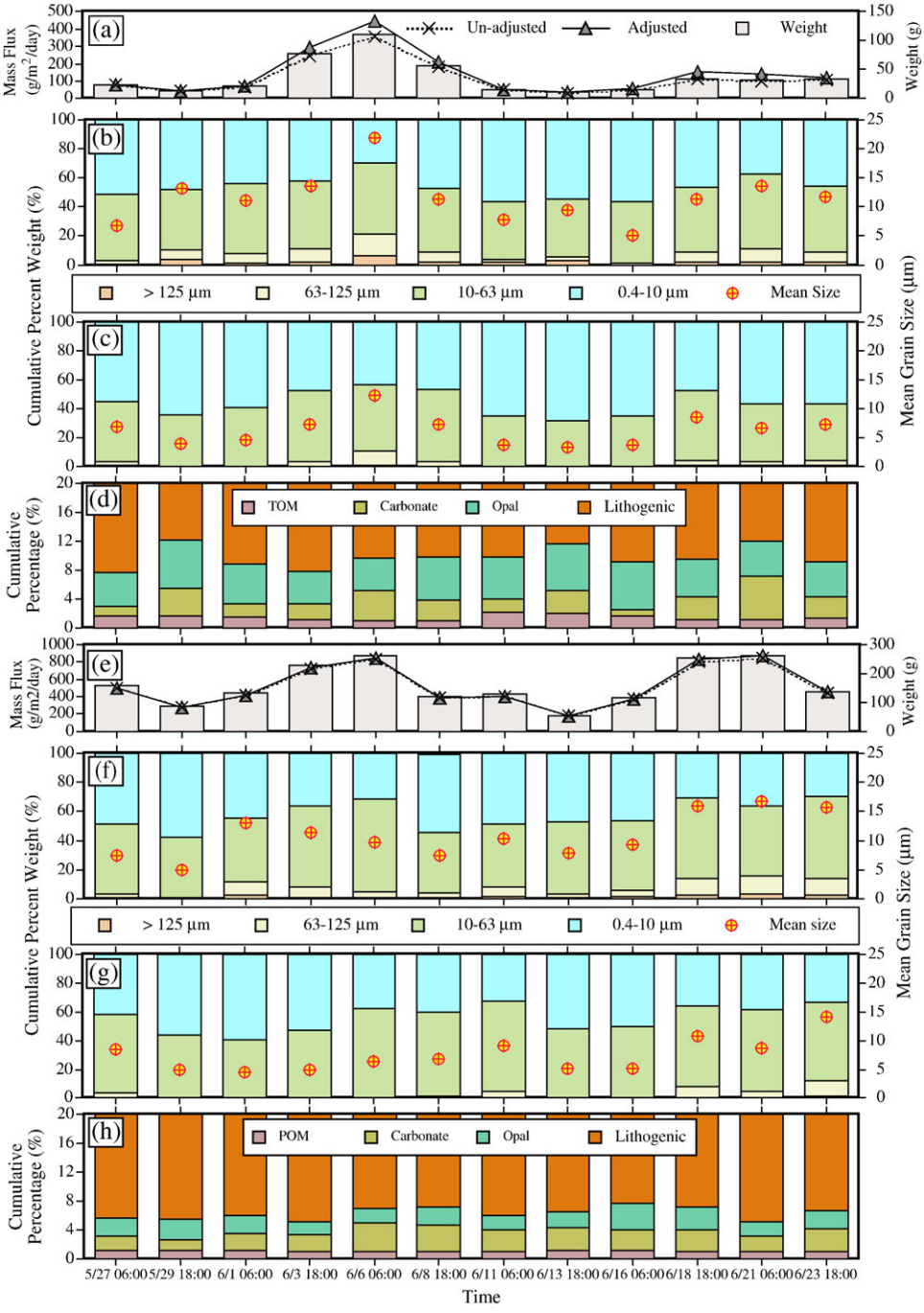

Fig. 4. Analysis results of the upper (a–d) and lower (e–h) sediment trap samples including the collected dry weight, adjusted (solid curve) and unadjusted (dashed curve) mass fluxes (a, e); cumulative percentage of 4 size-classes and the mean grain size of the 'untreated' (b, f) and 'treated' (c, g) samples; and the cumulative percentage (shown up to 20%) of the three nonlithogenic components (d, h).

upper rim, the fluxes were smaller (Fig. 4e). In general, fluxes at the deeper part of the canyon were between 2 and 7 times greater that those at the upper rim of the canyon. The signals of the two spring tides are clearly shown in the fluxes of lower trap, yet only the first spring tide is reflected in the upper trap. This might have to do with the irregular shore-normal flow pattern during the second spring tide (Fig. 3a). The difference in particle fluxes suggests that suspended particles in the deeper part of the canyon cannot all come from downward settling, and lateral transport is important in deeper part of the canyon.

Based on the particle-size compositions of the sediment trap samples, the collected particles in the KPSC are predominantly fine-grained (clay to fine silt) material (Fig. 4b, f). The collecting cups corresponding to the two spring tides (June 6 and 21) had greater coarse fraction. The total percentages of the three nonlithogenic components were higher at the upper rim than at the lower part of the canyon (Fig. 4d, h). They were also subject to greater temporal fluctuations at the upper rim. The biogenic opal in the lower part of the canyon had the greatest reduction then the other

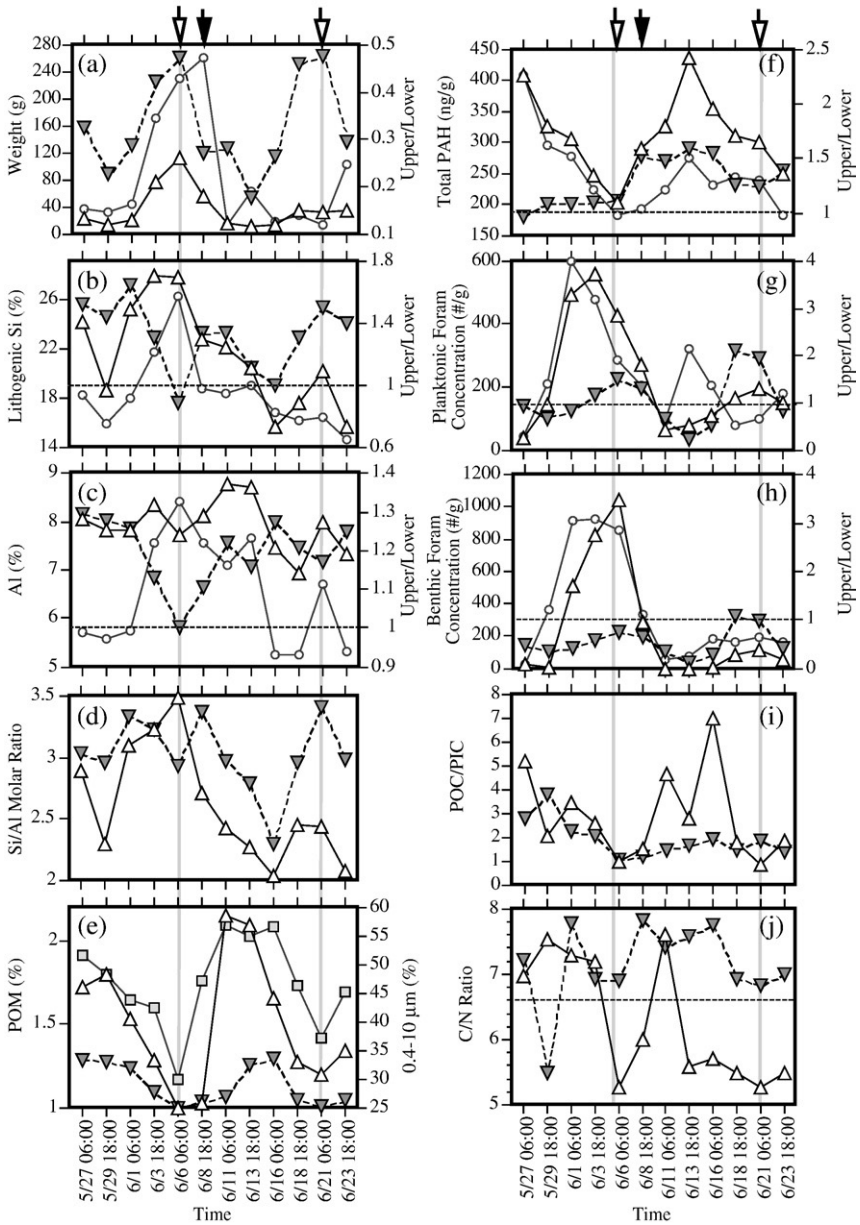

Fig. 5. Contrast between the collected particles in the upper and lower traps in terms of (a) total dry weight, (b) lithogenic silica (Si), (c) lithogenic aluminum (Al), (d) Si/Al molar ratio, (e) POM and the percentage of the 0.4–10 μm size-class (squares), (f) total PAH, (g) planktonic foram concentration, (h) benthic form concentration, (i) POC/PIC ratio, and (j) C/N ratio, the Redfield ratio (6.6) is indicated by the dashed line. The open triangles indicate the upper trap, the full inverted triangles indicate the lower trap, and the circles are the ratios between the values in the upper and the lower traps. The two hollow arrows point to the time points corresponding to the spring tides on 6/6 and 6/21 and the black arrow points to the time of maximum local influence of Typhoon Conson on 6/8.

Table 2
Linear regression analysis results (r^2, p) among alongshore flow and measured variables in the upper trap

Variables	r^2	p
Dry weight	+0.71	0.0006
Percentage of 63–125 μm	+0.66	0.0004
Percentage of 0.4–10 μm	−0.59	0.00036
Planktonic foram concentration	+0.68	0.0011
Benthic foram concentration	+0.72	0.0004
Total PAH	−0.69	0.0008
POM	−0.57	0.00045

Note: The relation is statistically significant if p is less than 0.05. '+' indicates positive relation, '−' indicates negative relation.

two. After removing the three nonlithogenic components from original samples, their mean size became finer (Fig. 4c, g) mainly due to the reduction of the two coarsest size-classes, suggesting nonlithogenic substances are associated with coarser particles.

The peak in the upper/lower trap weight ratio at June 8 corresponds to the high input from wave-related shelf resuspension at the canyon rim during Typhoon Conson (Figs. 2b, 5a) similar to what Liu and Lin (2004) observed during another typhoon. When one visually compares the temporal variations of the mass flux (collected weight) and size-composition of the raw samples (Fig. 4a, b) in the upper trap, there seems to be a link between the increased weight with increased percentage of the coarse fractions (>63 μm) especially at the time of the first spring tide on June 6. A linear regression analysis that followed shows that in the upper trap, the collected dry weight has positive and highly significant ($p<0.01$) correlation with the 63–125 μm size-class ($r^2=0.68$, $p=0.0013$); and negative correlation with the 0.4–10 μm size-class ($r^2=-0.60$, $p=0.0032$). This suggests that the 63–125 μm size-class contributed significantly to the increase of the collected weight of the particles in the upper trap and the negative relation is an artificial effect of the closed system (total sum of percentages has to be 100). In the lower trap, the only significant linear correlation (negative) exists between the collected weight and the percentage of the 0.4–10 μm size-class ($r^2=-0.54$, $p=0.0064$). This indicates that particles other than the 0.4–10 μm size-class contributed to the collected weight without one size-class being the dominant contributor.

5.2.2. Lithogenic silica, aluminum, and Si/Al molar ratio

Generally, at the upper rim, the lithogenic silica follows the trend of the total weight of the sediment trap (Fig. 5a, b). In the lower part of the canyon, no secular trend exists between the particle weight and lithogenic silica.

However, the percentage of lithogenic silica is higher at the upper rim than near the bottom of the canyon only during the first spring tide as shown by the greater than unity value of the upper/lower ratio (Fig. 5b). One likely explanation is that the spring tide was the most important transport agent that brought extraordinary amount of lithogenic silica to the upper canyon (Figs. 2c, 4a, and 5b). The ratio is less than unity for the rest of the record since the traps behaved normally that more lithogenic particles were always collected in the lower traps than in the upper traps in coastal and marginal seas (Monaco et al., 1990; Hung et al., 2003).

The percentage of lithogenic aluminum is generally higher at the upper rim than near the bottom of the canyon (Fig. 5c) suggesting the upper rim is closer to the terrestrial sources of the lithogenic aluminum. Furthermore, at the first spring tide, lithogenic Al also had high values, resulting in a high upper/lower ratio at this time point. The same explanation for the lithogenic Si can be applied to the Al variations.

Except for one time point at the first spring tide, the Si/Al molar ratios at the lower part of the canyon are greater than those at the upper rim (Fig. 5d). The higher than 2 values of Si/Al ratio are likely caused by the strong influence of non-clay minerals (layer Al-silicates), such as quartz and feldspars, etc. Therefore, the ratios at the lower trap being greater than those at the upper trap may indicate that the lower trap collected more primary minerals. However, the temporal patterns of Si/Al molar ratios follow closely those of the collected weights at both traps. This suggests that the stronger tide (spring tide) deliveries more terrestrial lithogenic particles to the canyon, leading to the collection of more primary minerals.

5.2.3. POM

POM at the upper rim and deeper part of the canyon both shows the low values at the time of the two spring tides (Fig. 5e). A closer examination shows POM at the upper rim is closely associated with its carrier, the finest size-class (0.4–10 μm) (Fig. 5e). However, this relation is not clear for the POM in the lower trap. The POM-0.4–10 μm association is quantified by the linear regression, which shows $r^2=0.63$, $p=0.0032$ for the upper trap; $r^2=0.36$, $p=0.04$ for the lower trap.

Spring tides deliver more terrestrial particles, leading to smaller POM values due to the dilution effect (Liu et al., 2006). During the typhoon at June 8, POM in the upper trap was reduced by the increased amount of reworked siliciclastic sediment resuspended off the shelf by the higher wave energy despite of the higher percentage of the 0.4–10 μm size-class (Fig. 5e).

5.2.4. PAH

The total PAH shares similar patterns as the POM, showing lowest values at the first spring tide, and higher concentrations in the upper trap (Fig. 5f). The fact that the PAHs did not decrease during the time of Typhoon Conson, nor the upper/lower ratios have the second low value around the second spring tide suggest that the PAHs are subject to a wider range of source/process-related factors than POM. Nevertheless, the PAH pattern of samples collected during this period does exhibit some typical characteristics which could very likely be related to typhoon effects. Compared with those found before and after the typhoon, the upper trap collected particulates

Table 3
Linear regression analysis results (r^2, p) among the along-canyon flow (in 150° orientation) and measured valuables in the lower trap

Variables	r^2	p
Dry weight	+0.58	0.0041
Percentage of 0.4–10 μm	−0.55	0.006
Planktonic foram concentration	+0.52	0.0079

Note: The relation is statistically significant if p is less than 0.05. '+' indicates positive relation, '−' indicates negative relation.

bore minimal contribution from resuspension of bottom sediment. It was also found that this sample was collected during a shift in flow directions (seaward to landward, Fig. 3). The pattern of PAH for this sample is characterized by both petroleum origin (characteristics of terrestrial particles) and pyrolysis origin (characteristics of marine particles). In the same time, the source of the lower trap sample had much stronger pyrolysis signal than all others. The total PAH in the upper trap also has strong and significant linear relation with the finest size-class (r^2=0.58, p=0.0039).

5.2.5. Planktonic and benthic foram

The presence of benthic foraminiferal shells in sediment traps was reported in our previous deployment (between June 20 and July 20 in 2000; Lin et al., 2005). Generally, the species found in this deployment are more diverse and richer in taxa (38) than in the previous deployment (11 taxa). Nevertheless, numbers of species found in the lower trap are all significantly greater than those corresponding cups in the upper trap, consistent with the hypothesized lateral and/or up-canyon particle transport (Lin et al., 2005; Liu et al., 2006).

Planktonic and banthic forams have similar temporal patterns in the actual concentration and upper/lower ratio. Their concentrations are generally higher in the upper trap than in the lower trap (Fig. 5g, h). In the first half of the experiment, the concentrations of both types of forams in the upper trap were much higher than those in the lower trap and also, there were higher concentration of the benthic forams than the planktonic ones during this period. There are visual similarities between the upper/lower ratios of the collected weight (Fig. 5a) and the planktonic (Fig. 5g) and benthic (Fig. 5h) foram concentrations. Linear regression analysis revealed that in the upper trap, the collected weight is significantly correlated with the planktonic (r^2=0.46, p=0.015) and benthic (r^2=0.71, p=0.0006) forams.

In the lower trap, the planktonic forams have strong correlation with the collected weight (r^2=0.77, p=0.0002) and the benthic forams have marginal linear relation with the weight (r^2=0.34, p=0.047). These statistics suggest that biogenic particles such as forams are important components of the sinking particles in the submarine canyon.

5.2.6. POC/PIC

The POC to PIC ratios for all the collecting cups are all above the unity for both upper and lower traps (Fig. 5i). However, the ratios at the upper trap are mostly higher than those in the lower traps. Since biogenic particles coming from in-situ production in nutrient-rich coastal waters have higher POC/PIC; those with forams have low POC/PIC values; and those from terrestrial inputs also have lower POC/PIC values; the observed values of POC/PIC are likely the combined results of the mixture of all the above three resources.

5.2.7. C/N ratio

The C/N ratios range between 5 and 8, suggesting dominant marine over terrestrial sources (Masque et al., 2003). However, C/N ratios are mostly higher at the lower part of the canyon than at the upper rim indicating degradation and decomposition of organic matter as they settling through the water column (Masque et al., 2003; Lund-Hansen et al., 2004, Fig. 5j). Particles

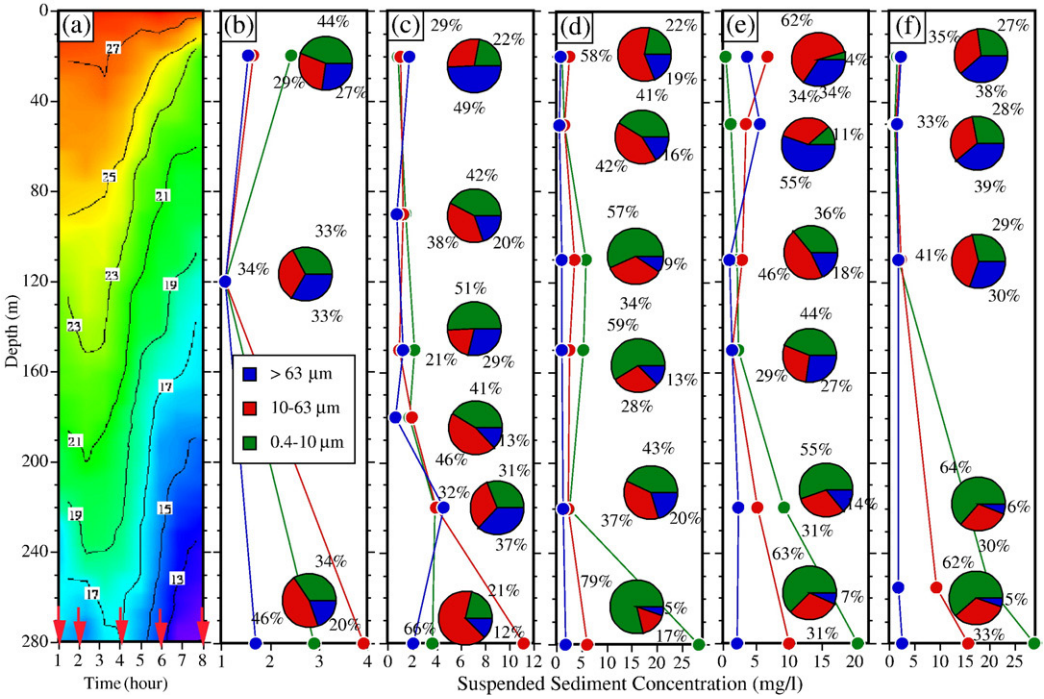

Fig. 6. (a) The temporal change of the vertical temperature structure during the 8-hour profiling experiment at St. N. The red arrows point to the hours at which the LISST-100 profiling (not shown) and water sampling were conducted. (b)–(f) Sequential plots of vertical distributions of the suspended sediment concentration (in mg/l) of three size-classes (>63, 10–63, and 0.4–10 µm) measured by filtration of water samples at hours 1, 2, 4, 6, and 8, respectively. At each sampling depth the pie diagram represents the percentages of the three size-classes.

coming from the Gaoping (Kaoping) River have C/N less than 9.0 (Hung, J.-J., unpublished data), largely resulted from a strong influence of anthropogenic sources from the KPR. Particles produced in-situ usually have lower C/N ratios, which explains the largely lower C/N values in the upper trap. Also, particles in the lower trap carry stronger terrestrial signals, which explains why the C/N values are mostly higher than Redfield ratio in the lower trap.

5.3. Transport of various particles

Linear regression analysis was performed among the properties of the particles with the averaged alongshore component of the flow at the upper rim (Fig. 3b) and with the along-canyon component at deeper part of the canyon (Fig. 3c) to establish particle–transport relationship. Only statistically significant results ($p<0.05$) are presented (Tables 2, 3) and discussed below.

5.3.1. Alongshore transport at the upper rim of the canyon

The following parameters from the upper trap have statistically significant positive relations with average alongshore velocity: total dry weight, percentage of 63–125 μm size-class, and planktonic and benthic foram concentrations (Table 2). These associations suggest that at the upper rim of the canyon coarser particles (major contributors to the collected weight) and biogenic particles are transported by northwesterly (positive alongshore) flow. This implies that the forams were probably from distal sources (Lin et al., 2005) carried by the branch to Kuroshio (Fig. 3) as suggested by Liu et al. (2006).

On the other hand, the percentage of 0.4–10 μm, total PAH, and POM at the upper rim all have correlations with the negative alongshore velocity (SE flow), suggesting that they were transported in the SE direction. Since the Gaoping River is located NW of the sediment trap moorings (Fig. 1a), the SE transport implies that the total PAH and POM were probably from the more proximal terrestrial sources of the KPR.

5.3.2. Along-canyon transport near the canyon floor

Since the lower sediment trap mooring was located near the canyon wall at the location where the canyon thalweg turns from near E–W orientation to NW–SE orientation (Fig. 1a), the along-canyon flow was defined to be positive in the 60° orientation seaward of the turning point and positive in the 150° orientation landward of this point. No correlation exists with the flow in the 60° orientation. The correlations of parameters with the flow in the 150° orientation were not as good as at the upper trap. Two positive correlations exist between the seaward along-canyon flow (150° orientation) and total dry weight and the planktonic foram concentrations (Table 3). These results suggest that down-canyon flows brought the planktonic forams from the head to the lower trap. The negative correlation between the along-canyon flow (150° orientation) and the 0.4–10 μm size-class suggests the finest size-class was transported up-canyon from offshore (Table 3).

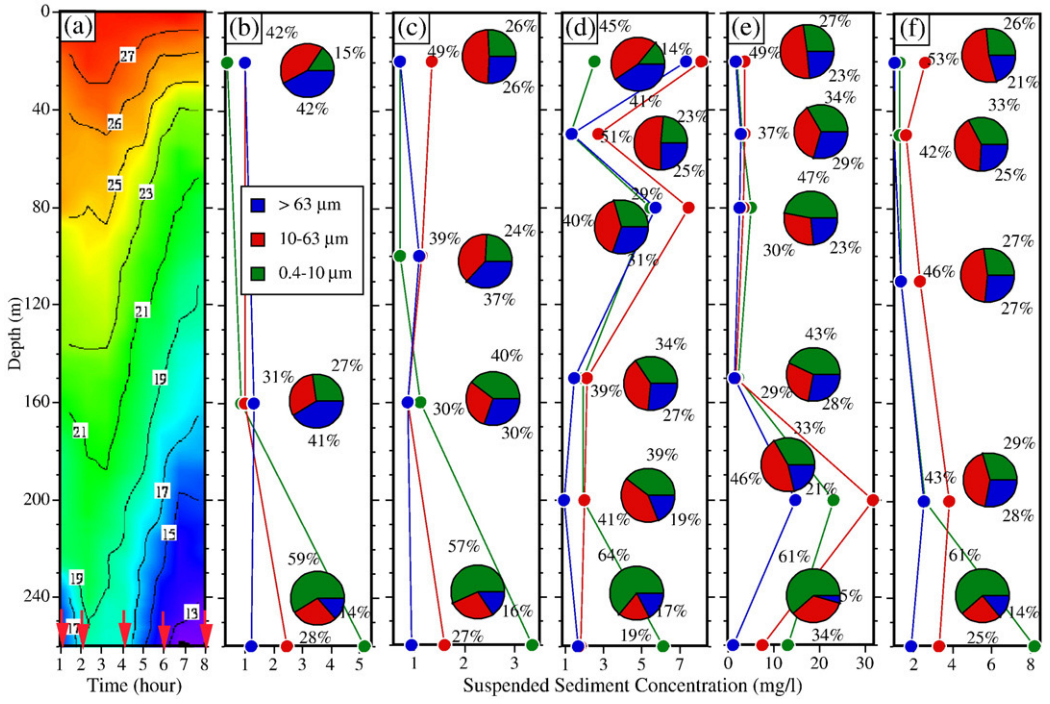

Fig. 7. (a) The temporal change of the vertical temperature structure during the 8-hour profiling experiment at St. M. The red arrows point to the hours at which the LISST-100 profiling (not shown) and water sampling were conducted. (b)–(f) Sequential plots of vertical distributions of the suspended sediment concentration (in mg/l) of three size-classes (>63, 10–63, and 0.4–10 μm) measured by filtration of water samples at hours 1, 2, 4, 6, and 8, respectively. At each sampling depth the pie diagram represents the percentages of the three size-classes.

5.4. Vertical variations of SSC and size-composition in the canyon water column

During the 8 hourly hydrographic profiling at St. N and M, only hours 1, 2, 4, 6, and 8 had water samples taken at various depths (Figs. 6, 7). The sampling period coincided with the tidal transition from down-canyon to up-canyon in the canyon interior as indicated by the temporal changes of the vertical temperature structures at N and M (Figs. 6a, 7a). During the ebb, the warmer coastal water filled the submarine canyon from the surface and flowed down-canyon as shown by the downward thickening of the warmer layers from the surface to the bottom of the canyon (Figs. 6a, 7a). When the tide changed from down-canyon to up-canyon between hours 3 and 4, colder offshore water was transported up-canyon and gradually filled up the canyon from below.

Except for the coarsest size-class (>63 μm), the SSC of the other two size-classes (0.4–10, 10–63 μm) show noticeable downward increase. The increase of the total SSC near the canyon floor indicates the existence of a BNL. The trend of downward increase is more pronounced in the finest size-class (0.4–10 μm). Consequently, the average percentage of this size-class increases from 22.7% in the surface water above the canyon to 56.0% in deeper part of the canyon (Figs. 6, 7). Conversely, the average percentage of the coarsest size-class decreases from 32.0% above the canyon to 12.0% in deeper part of the canyon. These trends suggest a downward fining of suspended sediment in the water column of the canyon. The vertical distributions of SSC look more 'erratic' at St. M (Fig. 7, d, e), which is probably caused by sediment entrainment from shelf substrate and canyon wall since this station was located near the canyon wall whereas St. N was located in the canyon's thalweg (Fig. 1). Since the measurements only spanned over 8 h, the data is circumstantial at this point to relate the semidiurnal tide with the settling of suspended sediment and BNL dynamics.

5.5. Core-to samples from the canyon floor

The sediment grain-size compositions in Cores #36, 37, and 32 (Figs. 8a, b; 9b) show that the substrate of the canyon floor is composed predominantly of hemipelagic mud (silt and clay). In Core #36, the exponential decrease of $^{210}Pb_{ex}$ activities with depth down-core suggest a steady sedimentation environment in which the accumulation of settling suspended particles is the primary process to form the subsurface strata (Fig. 8a).

Between 9 and 33 cm in the Core #37, there is a large interval of increased sand fraction (Fig. 8b). The marked decrease of $^{210}Pb_{ex}$ activities above 33 cm coincides with the abrupt increase of the sand faction. Above the 29 cm depth, the $^{210}Pb_{ex}$ activities resume the general increasing trend and yet are punctuated by fluctuations of smaller values at 21 and 4 cm depths (Fig. 8b). The down-core TOC values also show a large decrease between 33 and 28 cm depth and an anomalously high value at 23 cm depth. The down-core co-variations among the grain-size composition, $^{210}Pb_{ex}$ activities, and TOC suggest a major disturbances of the sedimentation occurred at the sharp boundary between 30 and 33 cm depths. Although no

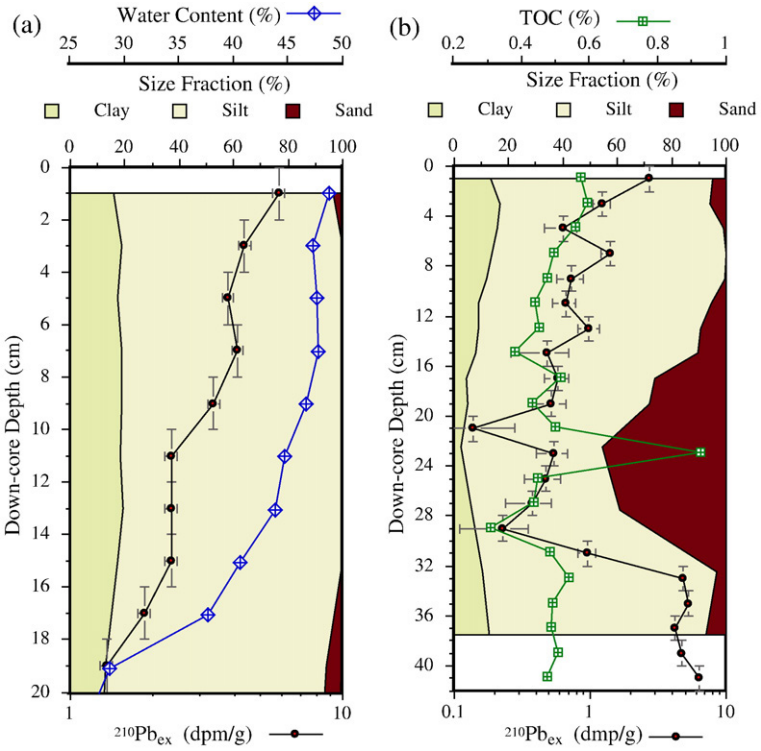

Fig. 8. Down-core measurements at St. 36 (a) including water content and $^{210}Pb_{ex}$ plotted over the cumulative percentage of clay, silt, and sand size-fractions; and (b) down-core measurements of TOC and $^{210}Pb_{ex}$ plotted over the cumulative percentage of clay, silt, and sand size-fractions at St. 37.

sedimentologic description is available for this core, the coarsening-up texture from 33–22 cm followed by fining-up texture from 23 cm to beyond 16 cm seem to suggest the presence of a hyperpycnite (Mulder et al., 2003), which could account for the anomalously high TOC at 23 cm. Yet, the general lack of vertical gradients in TOC and water content between 16 and 33 cm on the other hand, might suggest the effect of mixing during the erosion/deposition events.

Core #32 has more down-core information (Fig. 9). The down-core cumulative percentage of the three nonlithogenic components remains to be less than 6% of the total sediment (Fig. 9a). At the top of the core, the percentages of the three nonlithogenic components are similar to those in the lower sediment traps (Fig. 4h). When cross-comparing the lithogenic composition (Fig. 9a), the sand fraction (Fig. 9b), water content, TOC, and $^{210}Pb_{ex}$ activities, three anomalous layers located roughly between 5–8, 18–22, and 32–46 cm from the top of the core could be identified. Comparing to the 'background' hemipelagic mud, these layers generally have higher lithogenic composition; higher sand content; lower TOC, water content, and $^{210}Pb_{ex}$ activities (Fig. 9c). The layers of elevated sand fraction indicate graded bedding and alternate fining-up sequence, which is indicative of turbiditic deposits (Kudrass et al., 1998; Mulder et al., 2001). Since no sedimentologic description was made, we could not ascertain that classical Bouma sequences are present (Shanmugam, 1997).

6. Discussions

The observations and analysis results in this study cover a wide range of physical and biogeochemical processes that transcend time scales from episodic events, to tidal and subtidal, to time-averaged (beyond seasonal), and to centuries in the head region of the KPSC. In the following discussions, all the findings are integrated into a conceptual model for particle dynamics in a source-to-sink perspective with the emphasis on grain size for the study area (Fig. 10).

6.1. Delivery of fluvial, reworked, and biogenic particles to the submarine canyon

Although the river hydrological cycle determines the strength of the fluvial discharge by the KPR on the seasonal scale, it is the tides (especially the spring tide) that deliver the suspended particles discharged by the river to the submarine canyon (Fig. 3). The finest (finer than the very-fine silt) suspended particles in the river effluent are carried by the river plume on the shelf (Fig. 10A) whose dispersal is largely subject to the plume dynamics discussed by Liu and Lin (2004). Particles in the river effluent coarser than the very-fine silt descend into the submarine canyon modulated by the tides (Fig. 10B) (Liu et al., 2006). There is a greater diversity of suspended particles at the upper rim of the canyon. In addition to the lithogenic and nonlithogenic (organic) particles discharged by the river (proximal sources), there are reworked sediments resuspended off the shelf floor (Fig. 10C), and biogenic particles such as benthic and planktonic forams and particles related to the authigenic primary production (lower C/N ratio, Fig. 5j) on the shelf (Fig. 10C, D). Because of the proximity to the terrestrial sources, lithogenic Si, Al, POM, and PAHs have higher amount at the upper rim than at the deeper part of the canyon (Fig. 5b, c, e, f). The greater than unity values

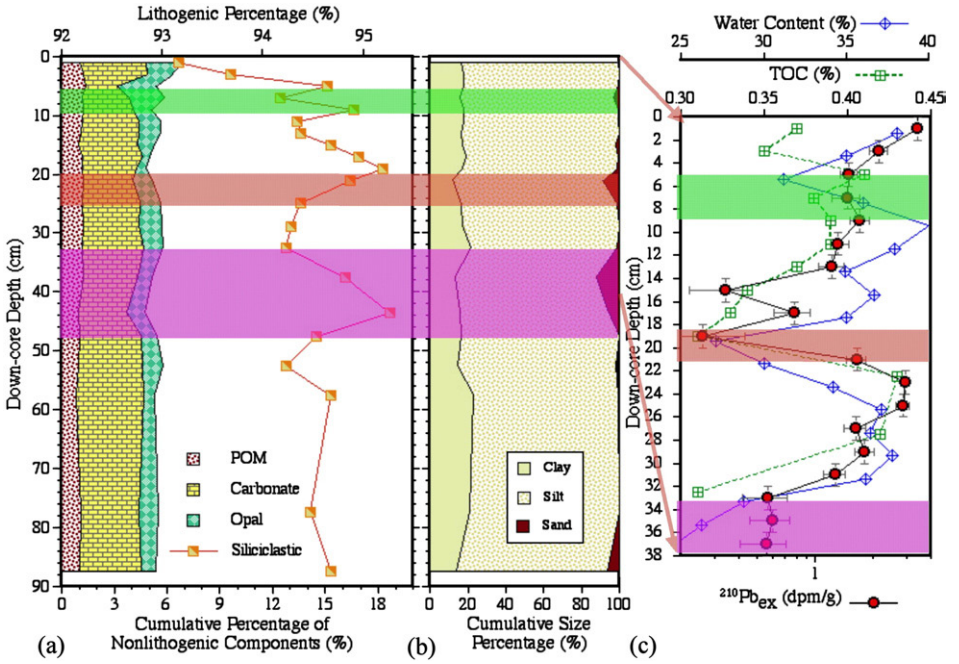

Fig. 9. Extensive measurements of the down-core properties for the box core at St. 32 including the cumulative percentage of the three nonlithogenic components and the percentage of the corresponding lithogenic fraction (a), the cumulative percentage of the three size-fractions (b), and for the top 38 cm of the core, the measurements of water content, TOC, and $^{210}Pb_{ex}$. Horizontal thick lines indicate three layers of disturbances in all the measurements at about 5–8, 18–22, and 32–46 cm from the top of the core.

for the upper-to-lower ratio in planktonic foram concentrations suggest that the upper rim of the canyon is closer to their pelagic habitats than the deeper part of the canyon (Fig. 5g, h). Yet, both the benthic and planktonic forms are transported on the shelf and slope to the study site from distal sources by the branch of northwesterly Kuroshio currents (Table 2).

6.2. Biogeochemical transformation of settling particles

The size of the suspended particles is an important factor affecting the physical and biogeochemical characteristics of the particles collected by the two sediment traps. For example, the size factor is illustrated by the mimicking relationship between the percentage of the finest size (0.4–10 μm) and POM (Fig. 5e). Since biogenic and nonlithogenic particles have greater presence at the upper rim of the canyon (Figs. 4, 5) and their sizes are larger (Fig. 5), as these particles settle through the water column of the canyon, physical and biogeochemical transformations take place. The smaller mean grain size of sediment samples in the lower trap suggest that as particles fall through the water column, they become finer. This fining process is associated with decreasing nonlithogenic signatures in the suspended particles as indicated by the lower POM and PAH concentrations near the canyon floor despite of the increase in the percentage of their preferred fine-grained carriers (Fig. 10E). Additionally, the lower POC/PIC ratio at the deeper part of the canyon is likely due to the increased decomposition of the organic carbon as particles fall through the canyon (Fig. 5i). On the other hand, the inorganic carbon remains in tact on the settling particles. The C/N ratio is higher near the canyon floor could be because of the preferentially decayed nitrogen as the particles settle and also because of stronger lithogenic signature. In addition to particles settling from above, periodic resuspension from the canyon floor, entrainment from the canyon walls, and along-canyon transport probably all contribute to form BNL (Fig. 10F). Planktonic and benthic forams form a significant source for biogenic particles in the deeper part of the canyon. They are fall-outs from above and are transported up-canyon from distal source on the slope and South China Sea basin (Fig. 10G).

6.3. Turbidity currents as an important mode of sediment transport in the canyon

The presence of turbiditic and hyperpycnite layers of post-depositional disturbances suggests occurrences of active erosion (Fig. 10H) and deposition processes from high SSC fall-out (Fig. 10I) on the submarine canyon floor. Erosion would remove younger layers of sediment and expose older sediment below, resulting in lower values of $^{210}Pb_{ex}$ activities in the core-top samples from the canyon. Erosion of the surface of the substrate could take the form of mass movement triggered by earthquakes (Huh et al., 2004; Sari and Cagatay, 2006) such as the canyon-wall slumping or slope failure; or the form of entrainment by turbidity currents triggered by earthquakes and typhoons (Xu et al., 2004; Liu et al., 2006). The deposition of eroded older sediment could create an 'overturned' deposit as indicated in Core #37, of which the top 29 cm thick of the sediments is older than those below (Fig. 8b).

Episodic events are probably frequent for the canyon environment as indicated by the presence of multiple 'disturbance layers' in Core #32 (Fig. 9). Each of these layers could represent episodes of erosion/deposition as compared to the background hemipelagic sediments. The high lithogenic composition, low $^{210}Pb_{ex}$ activities, TOC, and water

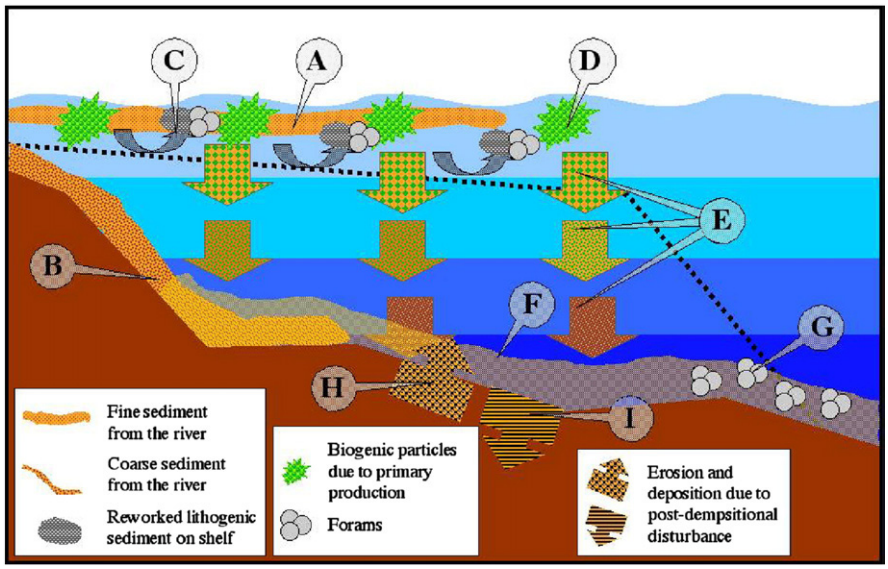

Fig. 10. The schematic plot of the conceptual model for the particle dynamics in the head region of the Gaoping Submarine Canyon. The thick dashed line depicts the upper and lateral boundaries of the canyon. The bands of different colors in the background represent the general stratification of the water column especially in the interior of the canyon. The first legend panel comprises particles from the fluvial and reworked shelf sources. The second panel represents particles of biogenic origins. The third panel includes processes related to post-depositional erosion (by turbidity currents) and deposition (hyperpycnites and turbidites). See text for the explanations of callouts A to I.

content in these layers probably indicate they are older than the background deposits. The higher percentage of sand in these layers is likely the result of reworking and transport and thus, older deposits.

6.4. Submarine canyon sediment transport and sedimentation

Material in the lower trap has similar composition to those in the upper trap, suggesting it also captured river-borne and resuspended material from the shelf. The close similarity in values of cumulative percentage of the three nonlithogenic components, the textural composition, and TOC between the samples in the lower trap and the core-top immediately below the lower sediment trap (in Core #32) suggests direct deposition of suspended sediment from the water above (Figs. 4, 5, 9). Yet the fact that the lower trap collected more particles than the upper trap (higher mass fluxes), and the suspended sediment mass concentrations are higher in the deeper part of the canyon suggest that the river and shelf only supply part of the suspended particles to the deeper part of the canyon. A certain percentage of the suspended particles in the deeper part of the canyon have to be transported laterally from offshore or from the head region of the canyon. The major evidence of offshore biogenic particles came from forams (Lin et al., 2005). Furthermore, the higher concentration in BNL and low nonlithogenic signatures of suspended particle in the deeper part of the canyon might be caused by the entrainment of canyon-wall slumping, turbidity currents, and boundary mixing. Terrestrial and shelf sediment once being delivered to the Gaoping Submarine Canyon might go through repeated cycles of deposition, erosion, and transport in their eventual down-canyon movement and burial.

7. Conclusion

This study presents analysis results of particles taken concurrently from the sediment traps, core-top, and water samples to form a conceptual model for particle dynamics and sedimentation in the Gaoping Submarine Canyon. In the head region of the KPSC particles from lithogenic sources dominate the suspended sediment at the upper rim (90.2%) and in the deeper part (93.6%) of the canyon. On the surface of the canyon floor, the lithogenic and biogenic compositions in the sediment are similar to those measured in the lower sediment trap, suggesting close coupling between the settling particles and canyon floor deposition. As particles fall through the submarine canyon interior, the average percentage of clay and fine silt (0.4–10 μm) increases with depth from 22.7% at the upper rim to 56.0% at the deeper part of the canyon. Associated with the fining trend in the settling particles, are the geochemical transformations as indicated by the downward decrease of the content of organic substances such as POM and PAH; the lowered POC/PIC ratio, and the increased C/N ratio due to differential decomposition, degradation, and remineralization. A benthic nepheloid layer (BNL) exists, whose concentration and thickness is closely related to the up-canyon flow of cold water from offshore. Settling particles from the river effluent, reworked shelf substrate, and biogenic processes in the upper part of the canyon cannot account for all the suspended particle downward fluxes near the canyon floor. Additional sources likely come from current resuspension, entrainment, and along-canyon advection of offshore sediment and rebound sediment. The presence of turbiditic and hyperpycnic deposits on the canyon floor indicates the canyon substrate might go through episodes of stepwise erosion and deposition due to earthquakes and typhoons, which might be significant modes of down-canyon sediment transport.

Acknowledgements

The funding for this study was provided by the R.O.C. National Science Council under grand numbers NSC 93-2611-M-110-013 and NSC 94-2611-M-110-002 to J.T. Liu; NSC 94-2611-M-110-016 to J.-J. Hung; NSC 94-2611-M-110-008 to H.-L. Lin; NSC 94-2611-M-001-002 and NSC 95-2611-M-001-002 to C.-A. Huh; and NSC 94-2611-M-110-020 to C.-L. Lee. We want to express our sincere gratitude to Dr. Guo-Wei Hung and his associates at the Sediment Trap Laboratory of the National Center for Ocean Research for their hard work in the design, assemblage, deployment, and retrieval of the sediment trap arrays. We are grateful to Peter Tsao's invaluable assistance in the field with the chartered boat operation and guarding the deployed instruments during the field experiment period. We thank Captain Wu and his officers and crew of R/V Ocean Researcher III for their assistance in the data acquisition. We also thank Jeff C. Huang, and Fanta Hsu for their help in the fieldwork and sample analysis. The Water Resources Bureau provided the hydrology data of Kaoping River, and the Central Weather Bureau provided the weather and wave data. We also want to thank two anonymous reviewers for their helpful suggestions and comments to improve the manuscript. Marilyn Ritzer-Liu proofread a later version of the manuscript.

References

Bonnin, J., van Raaphorst, W., Brummer, G.-J.A., van Haren, H., Malschaert, H., 2002. Intense mid-slope resuspension of particulate matter in the FAERoe-Shetland Channel: short-term deployment of near-bottom sediment trap. Deep-Sea Research I 49, 1485–1505.

Chung, Y.-C., Hung, G.-W., 2000. Particulate fluxes and transport on the slope between the southern East China Sea and the South Okinawa Trough. Continental Shelf 20, 571–597.

Fabres, J., Calafat, A., Sanchez-Vidal, A., Canals, M., Heussner, S., 2002. Composition and spatio-temporal variability of particle fluxes in the Western Alboran Gyre, Mediterranean Sea. Journal of Marine Systems 33–34, 431–456.

Gardner, W.D., 1989. Periodic resuspension in Baltimore Canyon by forcing of internal waves. Journal of Geophysical Research 94, 18185–18194 No. C12.

Granata, T.C., Vidondo, B., Duarte, C.M., Satta, M.P., Gracia, M., 1999. Hydrodynamics and particles transport associated with a submarine canyon off Blanes (Spain), NW Mediterranean Sea. Continental Shelf Research 19, 1249–1263.

Huh, C.-A., Su, C.-C., Liang, W.-T., Ling, C.-Y., 2004. Linkages between turbidites in the southern Okinawa Trough and submarine earthquakes. Geophysical Research Letters 31, L12304. doi:10.1028/2004GL019731.

Huh, C.-A., Su, C.-C., Wang, C.-H., Lee, S.-Y., Lin, I.-T., 2006. Sedimentation in the Southern Okinawa Trough—rates, turbidites and a sediment budget. Marine Geology 231, 129–139.

Hung, G.-W., Chung, Y.-C., 1998. Particulate fluxes, ^{210}Pb and ^{210}Po measured from sediment trap samples in a canyon off northeastern Taiwan. Continental Shelf Research 18, 1475–1491.

Hung, J.-J., Lin, P.-L., Liu, K.-K., 2000. Dissolved and particulate organic carbon in the southern East China Sea. Continental Shelf Research 20, 545–549.

Hung, J.-J., Lin, C.-S., Chung, Y.-C., Hung, G.-W., Liu, W.-S., 2003. Lateral fluxes of biogenic particles through the Mien-Hua canyon in the southern East China Sea slope. Continental Shelf Research 23, 935–955.

Khripounoff, A., Vangriesheim, A., Babonneau, N., Crassous, P., Dennielou, B., Savoye, B., 2003. Direct observation of intense turbidity current activity in the Zaire submarine valley at 4000 m water depth. Marine Geology 194, 151–158.

Ko, F.-C., Baker, J., Fang, M.-D., Lee, C.-L., 2007. Composition and distribution of polycyclic aromatic hydrocarbons in the surface sediments from the Susquehanna River. Chemosphere 66, 277–285.

Kudrass, H.R., Michels, K.H., Wiedicke, M., Suckow, A., 1998. Cyclones and tides as feeders of a submarine canyon off Bangladesh. Geology 26, 715–718 no. 8.

Lee, I.-H., Liu, J.T., 2006. Rectification of the heading and tilting of sediment trap arrays due to strong tidal currents in a submarine canyon. Geophysical Research letters 33, L08609. doi:10.1029/2005GL025183.

Leinen, M., 1977. A normative calculation technique for determining opal in deep-sea sediments. Geochimica et Cosmochimica Acta 41, 671–676.

Lin, H.-L., Liu, J.T., Hung, G.-W., 2005. Foraminiferal shells in sediment traps: implications of biogenic particle transport in the Kao-ping Submarine Canyon. Continental Shelf Research 25, 2261–2272.

Liu, J.T., Lin, H.-L., 2004. Sediment dynamics in a submarine canyon: a case of river–sea interaction. Marine Geology 207 (1–4), 55–81.

Liu, J.T., Liu, K.-j., Huang, J.C., 2002. The influence of a submarine canyon on river sediment dispersal and inner shelf sediment movements: a perspective from grain-size distributions. Marine Geology 181 (4), 357–386.

Liu, J.T., Lin, H.-L., Hung, J.-J., 2006. A submarine canyon conduit under typhoon conditions off Southern Taiwan. Deep Sea Research I 53, 223–240.

Lund-Hansen, L.C., Pejrup, M., Floderus, S., 2004. Pelagic and seabed fluxes of particulate matter and carbon, and C:N ratios resolved y sediment traps during a spring bloom, southwest Kattegat. Journal of Sea Research 52, 87–98.

Masque, P., Fabres, J., Canals, M., Sanchez-Cabez, J.A., Sanchez-Vidal, A., Cacho, I., Calafat, A.M., Bruach, J.M., 2003. Accumulation rates of major constituents of hemipelagic sediments in the deep Alboran Sea: a centennial perspective of sedimentary dynamics. Marine Geology 193, 207–233.

Miserocchi, S., Faganeli, J., Balboni, V., Heussner, S., Monaco, A., Kerherve, P., 1999. Characteristics and sources of the settling particulate organic matter in the South Adriatic basin. Organic Geochemistry 30, 411–421.

Monaco, A., Biscaye, P.E., Soyer, J., Pocklington, R., Heussner, S., 1990. Particle fluxes and ecosystem response on a continental margin: the 1985–1988 Mediterranean ECOMARGE experiment. Continental Shelf Research 10, 809–839.

Mortlock, R.A., Froelich, P.N., 1989. A simple method for the rapid determination of biogenic opal in pelagic marine sediments. Deep Sea Research I 36, 1415–1426.

Mulder, T., Weber, O., Anschutz, P., Jorrissen, F.J., Jouanneau, J.-M., 2001. A few months-old storm-generated turbidite deposited in the Capbreton Canyon (Bay of Biscay, SW France). Geo-Marine Letters 21, 149–156.

Mulder, T., Syvitski, J.P.M., Migeon, S., Faugeres, J.-C., Savoye, B., 2003. Marine hyperpycnal flows: initiation, behavior and related deposits. A review. Marine and Petroleum Geology 20, 861–882.

Mullenbach, B.L., Nittrouer, C.A., 2000. Rapid deposition of fluvial sediment in the Eel Canyon, northern California. Continental Shelf Research 20, 2191–2212.

Palanques, A., Khatab, M.E., Puig, P., Masque, P., Sanchez-Cabeza, J.A., Isla, E., 2005a. Downward particle fluxes in the Guadiaro submarine canyon depositional system (north-western Alboran Sea), a river flood dominated system. Marine Geology 220, 23–40.

Palanques, A., Garcia-Ladona, Gomis, D., Martin, J., Marcos, M., Pascual, A., Puig, P., Gili, J.-M., Emelianov, M., Monserrat, S., Guillen, J., Tintore, J., Segura, M., Jordi, A., Ruiz, S., Basterretxea, G., Font, J., Blasco, D., Pages, F., 2005b. General patterns of circulation, sediment fluxes and ecology of the Palamos (La Frontera) submarine canyon, northwestern Mediterranean. Progress in Oceanography 66, 89–119.

Puig, P., Palanques, A., Guillen, J., El Khatab, M., 2004. Role of internal waves in the generation of nepheloid layers on the northwestern Alboran slope: implications for continental margin shaping. Journal of Geophysical Research 109, C09011. doi:10.1029/2004JC002394.

Sanchez-Vidal, A., Calafat, A., Canals, M., Frigola, J., Fabres, J., 2005. Particle fluxes and organic carbon balance across the Eastern Alboran Sea (SW Mediterranean Sea). Continental Shelf Research 25, 609–628.

Sari, E., Cagatay, M.N., 2006. Turbidites and their association with past earthquakes in the deep Cinarcik Basin of the Marmara Sea. Geo-Marine Letters 26, 69–76.

Shanmugam, G., 1997. The Bouma sequence and the turbidite mind set. Earth Science Review 42, 201–229.

Timothy, D.A., Soon, M.Y.S., Calvert, S.E., 2003. Settling fluxes in Saanich and Jervis Inlets, British Columbia, Canada: sources and seasonal patterns. Progress in Oceanography 59, 31–73.

Xu, J.P., Noble, M.A., Rosenfeld, L.K., 2004. In-situ measurements of current structures within turbidity currents. Geophysical Research Letter 31, L09311. doi:10.1029/2004GL019718.